ADVANCED FUNCTIONAL MATERIALS

www.afm-journal.de

Plasmon-Enhanced Photodetection in Ferromagnet/Nonmagnet Spin Thermoelectric Structures

*Chul-Yeon Jeon, Kwang Min Baek, Shinho Kim, Dong-Jun Kim, Min Seok Jang, Yeon Sik Jung, and Byong-Guk Park**

The photothermoelectric (PTE) effect that originates from the temperature difference within thermoelectric materials induced by light absorption can be used as the mechanism for a light sensor in optoelectronic applications. In this work, a PTE-based photodetector is reported using a spin thermoelectric structure consisting of CoFeB/Pt metallic bilayers and its signal enhancement achieved by incorporating a plasmonic structure consisting of Au nanorod arrays. The thermoelectric voltage of the bilayers markedly increases by 60 ± 10% when the plasmon resonance condition of the Au nanorods is matched to the wavelength of the incident laser. Full-wave electromagnetic simulations reveal that the signal enhancement is due to the increase in light absorption and consequential local heating. Moreover, the alignment of the Au nanorods makes the thermoelectric voltages sensitive to the polarization state of the laser, thereby enabling the detection of light polarization. These results demonstrate the feasibility of a hybrid device utilizing plasmonic and spin-thermoelectric effects as an efficient PTE-based photodetector.

1. Introduction

A temperature difference across conducting materials results in a voltage in an open-circuit condition due to the Seebeck effect. The thermally generated voltage is proportional to the Seebeck coefficient S of the material and temperature difference ΔT. When the temperature difference is developed optically, the capability to transduce optical signals to electrical signals via the mediation of thermoelectricity, called the photothermoelectric (PTE) effect, can be utilized for photodetection.[1–5]

To realize an efficient PTE photodetector of this kind, there are two primary requirements. The first is a sufficiently high heat-to-electricity conversion efficiency or a large thermoelectric figure of merit $ZT = \sigma S^2 T/\kappa$ where σ is the electrical conductivity, κ is the thermal conductivity, and T is the absolute temperature. The enhancement of ZT is limited by the interrelation of the two conductivities (σ and κ); thus, considerable effort has been devoted to decouple them via electronic structure modifications or the reduction in lattice thermal conductivity using phonon scattering.[6,7] Moreover, alternative approaches to enhance the thermoelectric efficiency have been studied in various materials.[8–11] Among them, the spin thermoelectric effect utilizes the thermoelectricity in magnetic multilayers,[11] which has the advantages over the conventional Seebeck effect such as a simple device structure, scaling competence, and possibility to control electrical and thermal conductivities independently.[12,13] This effect is employed in the PTE device proposed in this study. The second requirement for an efficient PTE photodetector is a strong light absorption capability. This can be realized by incorporating a plasmonic nanostructure that confines light within the structure in a resonance condition, thereby enhancing the light absorption significantly. Previous studies have shown an increased light absorption within the active layer of solar cells by introducing plasmonic nanostructures.[14–16] This approach has the advantage of wavelength- or polarization-sensitive absorption, allowing the control of the light absorption by tailoring the structural parameters of the nanostructures.[17–21] Moreover, the heat-energy dissipation from the plasmon resonance, known as plasmon-induced heating,[22–24] can enhance the thermoelectric voltage generation in PTE devices.

In this work, we demonstrate plasmon-enhanced photodetection in spin thermoelectric devices with CoFeB/Pt structures by integrating an Au nanorod array as a plasmonic absorber. We report a significant enhancement in spin thermoelectric voltage (60 ± 10%) based on the plasmon resonance of Au nanorods excited by laser illumination. Full-wave simulations using the finite element method suggest that the enhancement in the thermoelectric voltage is due to the increase in optical absorption of the CoFeB/Pt bilayers and resulting plasmon-induced local heating. This work demonstrates a novel approach to design a PTE-based photodetector using ultrathin spin thermoelectric layers with a plasmonic absorber.

C.-Y. Jeon, Dr. K. M. Baek, Dr. D.-J. Kim, Prof. Y. S. Jung, Prof. B.-G. Park
Department of Materials Science and Engineering
KAIST
Daejeon 34141, Republic of Korea
E-mail: bgpark@kaist.ac.kr
S. Kim, Prof. M. S. Jang
School of Electrical Engineering
KAIST
Daejeon 34141, Republic of Korea

The ORCID identification number(s) for the author(s) of this article can be found under https://doi.org/10.1002/adfm.201802936.

DOI: 10.1002/adfm.201802936

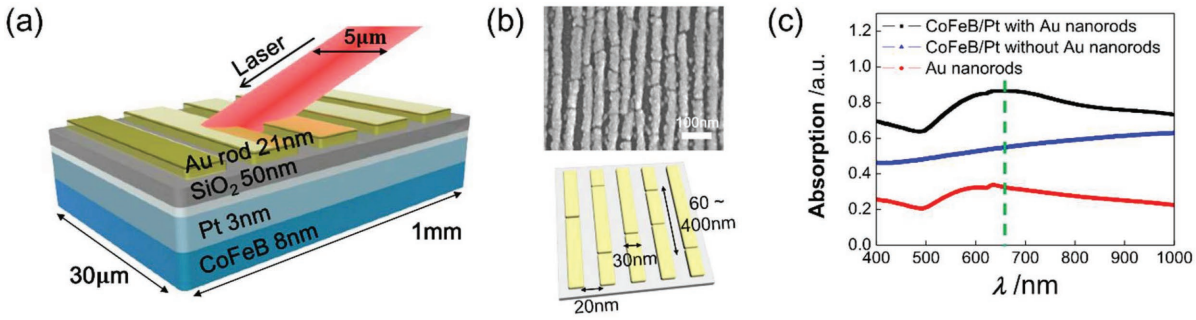

Figure 1. Plasmon-enhanced spin thermoelectric device. a) Schematic representation of the device consisting of a spin thermoelectric CoFeB/Pt bilayers and Au nanorod arrays. Here, the diameter of laser spot is 5 μm. b) SEM image of Au nanorod arrays. c) Optical absorption spectra of CoFeB/Pt layers with (black) and without (blue) an Au nanorod array on a glass substrate, together with a sample consisting of an Au nanorod array on a glass substrate (red). The green dotted line indicates the wavelength λ of the laser (660 nm) used in the thermoelectric measurement.

2. Results and Discussion

Figure 1a shows a schematic representation of the device structure, which consists of a spin thermoelectric CoFeB (8 nm)/Pt (3 nm) bilayers and a plasmonic nanostructure of Au nanorods. The Au nanorods that were formed on the stack through the solvent-assisted nanotransfer method,[25,26] have ≈30 nm in width and 50–400 nm in length, and the spacing between nanorods is 20 nm (Figure 1b). We note that a 50 nm SiO_2 layer was inserted between the CoFeB/Pt bilayers and the Au nanorods to improve plasmonic excitation.[27] Figure 1c shows the optical absorption spectra of the different samples on a glass substrate, where the black and blue lines represent the spectra of the CoFeB/Pt structures with and without an Au nanorod array, respectively, and the red line denotes the spectrum of Au nanorods alone. The broad absorption peak around 660 nm indicates the localized plasmon excitation of Au nanorods. Note that the slight dip of the absorption spectra at 630 nm is due to a technical error of the instrument when the light source is switched.

We first examine the PTE in CoFeB/Pt samples by using a linearly polarized laser with a wavelength of 660 nm. **Figure 2**a illustrates the schematic representation of the PTE voltage measured using two contact pads. The thermal gradient in the CoFeB/Pt bilayers induces a spin current that flows from the CoFeB layer into the Pt layer, in which the spin current converts into an electric voltage via the inverse spin Hall effect.[13,28] Figure 2b shows the PTE voltages as a function of magnetic field along the x-direction, H_x, demonstrating that the sign of the PTE voltage is changed upon the reversal of magnetization. In addition, Figure 2c shows the dependence of the PTE voltage on laser power, which indicates a linear increase in the PTE voltage with laser power and, thereby, temperature gradient. These results confirm that the PTE voltage originates from the spin thermoelectricity as the spin thermoelectric voltage (ΔV) is generated by the laser-induced temperature gradient (∇T) via the spin Seebeck effect and anomalous Nernst effect as $\Delta V \sim M \times \nabla T$, where M is the magnetization vector.[29,30] In our sample geometry, under a vertical temperature gradient ∇T_z, the signal along the y-direction, V_y, is maximized when M is aligned to the x-direction, as shown in Figure 2b. Under this condition, we study the effect of the plasmonic structure on the PTE voltage. By introducing Au nanorods on top of the CoFeB/Pt sample, the PTE voltage signal is significantly enhanced by 60 ± 10% (blue symbols in Figure 2b,c). Note that the resonance peak of the Au nanorods is close to the laser wavelength. We performed the same measurement using a laser with a wavelength of 830 nm (red symbols in Figure 2b), which is far from the resonance absorption peak of the Au nanorods (see black line in Figure 1c). Since the wavelength of the laser is not matched to the resonance condition of the Au nanorods, the light absorption and resultant signal is not considerably enhanced. This result demonstrates the critical role of the plasmon resonance effect in the voltage enhancement. We note that this enhancement can be also achieved in other structure of CoFeB/W bilayers (see Figure S1 in the Supporting Information).

Next, we present the capability of our device to detect the state of light polarization. In order to prove the concept, we introduce well-aligned Au nanorods that are coated on the bilayers in the direction perpendicular (PERP) or parallel (PARA) to the longer axis of the device, as illustrated in **Figure 3**a. We measured the PTE voltage V_y for the samples with the PERP and PARA alignments as well as a control sample without Au nanorods as a function of magnetization angle θ with respect to the x-direction on the x–y plane. Here, a magnetic field of 1000 Oe was used to rotate the magnetization and the linear polarization of the laser (or its electric field) was aligned to the longer axis of the device. Figure 3b shows that the signal enhancement only appears in the sample with the PERP alignment. To check the relation between the light polarization and rod alignment, we repeated the same measurement after rotating the samples by 90°, and the results in Figure 3c show an increase in the signal only for the sample with the PARA alignment. This clearly demonstrates that the enhancement in the PTE signal occurs when the electric-field component of the light is aligned to the shorter axis of the Au nanorods; in other words, the enhancement occurs when the transverse plasmon resonance condition of the Au nanorods is satisfied. Note that the phase shift of the PTE voltages in Figure 3c is due to the rotation of the sample; V_x is maximized when **M** is aligned to the y-direction ($\theta = 90°$).

The polarization dependence of the PTE signal is confirmed by an independent measurement, in which the light polarization is modulated using a wave plate while measuring the thermoelectric voltage and reflected laser power. **Figure 4**a shows

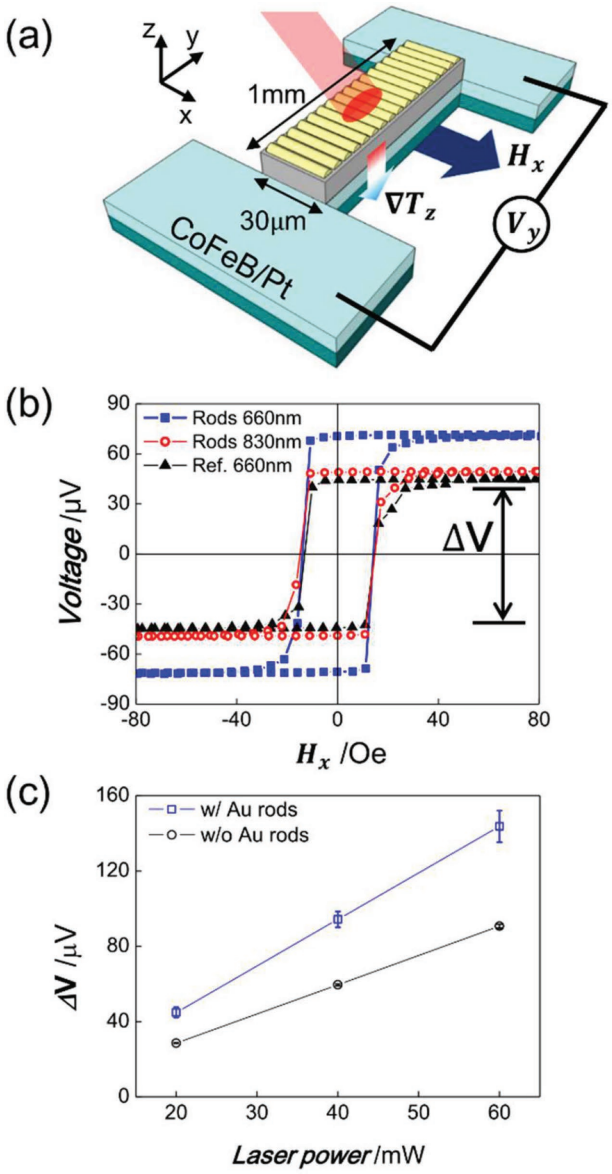

Figure 2. Plasmon-enhanced PTE voltage. a) Schematic representation of the PTE voltage measurement. A temperature gradient of CoFeB/Pt in the *z* direction (∇T_z) is generated upon laser illumination. b) The thermoelectric voltage versus magnetic field along the *x*-direction for the CoFeB/Pt sample with (blue) and without (black) Au nanorods. Here, the laser wavelength is 660 nm. The red symbols represent the result for CoFeB/Pt with Au nanorods, but at a laser wavelength of 830 nm. c) The thermoelectric voltage ΔV versus incident laser power. Here, ΔV is defined as $V(H = 80\ \text{Oe}) - V(H = -80\ \text{Oe})$. The error bar represents the standard deviation of 99% confidence interval.

the results, demonstrating a clear dependence of the PTE voltage ΔV on the polarization angle φ; maximum values are obtained when the transverse component of the polarization of light is at largest to satisfy the transverse plasmon resonance. These results are consistent with the results presented in Figure 3. Furthermore, Figure 4b shows the simultaneously measured reflected laser power that is minimized (maximized) for the φ value at which the PTE signal is the largest (smallest). These results indicate two points of interest. One is that the PTE signal can be controlled by the modulation of the light polarization, facilitating the use of our device as a polarization detector. The second is that the enhancement in the PTE signal is closely related to the increase in the light absorption under the transverse plasmon resonance condition.

To gain insight into the signal enhancement and its polarization dependency, we performed full-wave electromagnetic simulations using both the finite element method (COMSOL Multiphysics) and the finite difference time domain method (Lumerical FDTD) to obtain spatially resolved heat production profiles resulting from the absorption of incident light. By using the heat generation profiles as input parameters, we calculate temperature profiles in the samples by numerically solving heat transfer equations using the finite element method. The schematic representation of the layer structure used for the simulations is shown in **Figure 5**a. The optical and thermal properties of the materials and further details of the simulations are described in the Supporting Information. Figure 5b shows the simulated heat generation profiles ($\dot{Q}$) for two different incident light polarizations. When the light is polarized along the rods, the system does not show any signature of resonant behavior. On the other hand, the light polarization perpendicular to the rods induces a strong plasmonic resonance, thus increasing the light absorption significantly in the metallic nanorods. The light trapping effect due to the plasmonic resonance of the metallic nanorods is more clearly captured in the electric-field profile shown in Figure S1 in the Supporting Information. As a result of the strong plasmon resonance, light polarized perpendicular to the rods creates a temperature gradient in the CoFeB/Pt bilayers ≈2.7 times greater than light polarized parallel to the rods, as shown in Figure 5c. This result suggests that plasmon-induced heating should be the main cause of the PTE enhancement. We note that the temperature increase is somewhat larger than that in ΔV signal, which might be due to the uncertainty of material parameters for simulations, which we obtained from the literatures. Moreover, a perfect interface is assumed in the simulation, which however is not the case for the multilayered samples. This can reduce the light absorption in the active CoFeB/Pt bilayers. We also found that the simulated cell size or the air convection does not alter the calculated result of temperature profile (see Figure S3 in the Supporting Information). It has been reported that the spin thermoelectric voltage can be enhanced by plasmonic spin pumping[31]; however, such an effect might be negligible in our sample because of the thick SiO_2 layer between the Au nanorods and CoFeB/Pt bilayers. While the results are based on the focused illumination, our device can operate in a large area illumination by incorporating a localized plasmonic pattern and/or introducing spin thermopiles (see detail in the Supporting Information).

3. Conclusion

We demonstrated enhanced photodetection in a spin thermoelectric device by integrating a plasmonic structure consisting of Au nanorods. We observed a significant increase in the PTE voltage when the wavelength and polarization of the

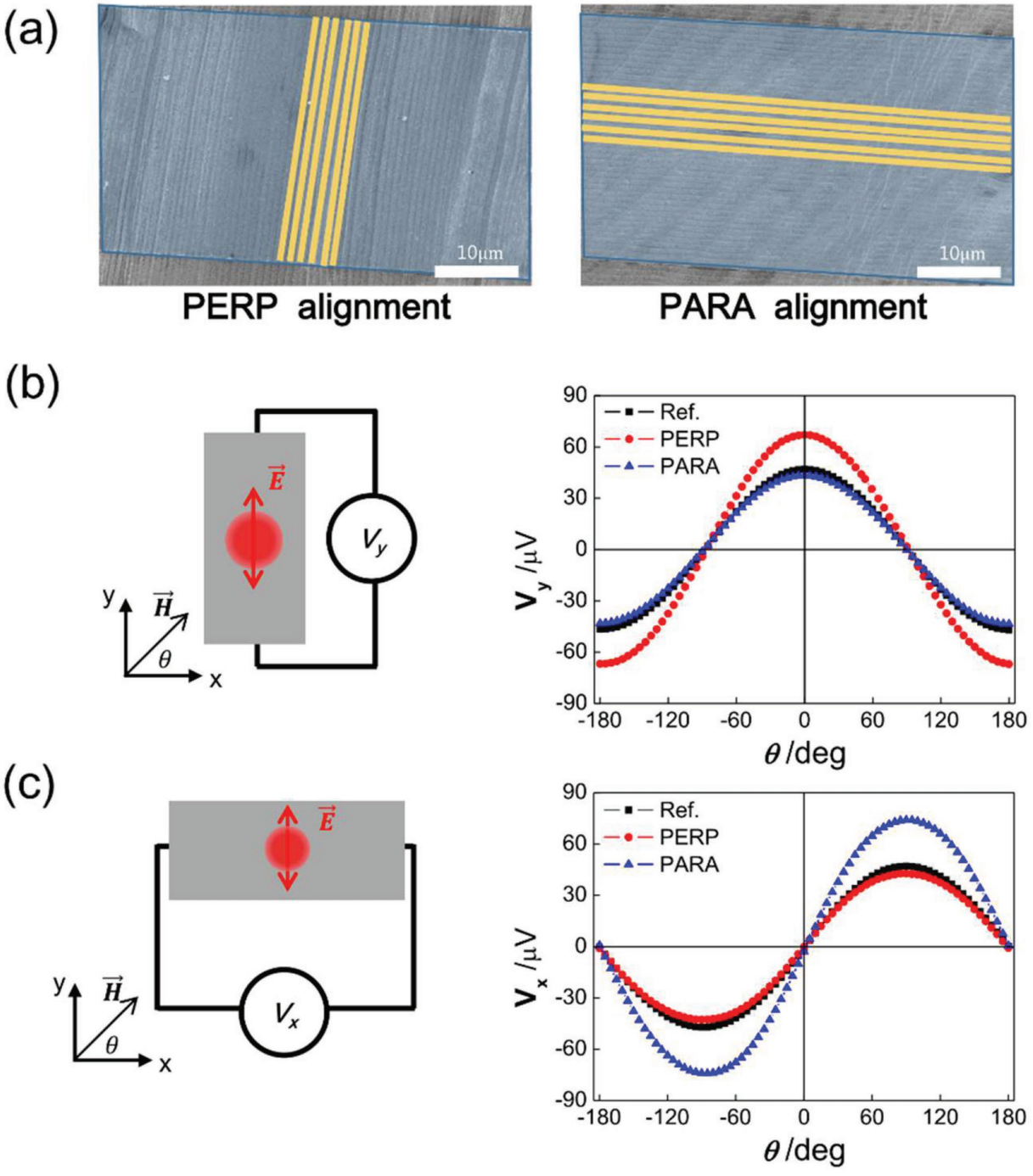

Figure 3. Dependence of the PTE voltage on the alignment of Au nanorods. a) SEM images of two different Au nanorod alignments with respect to the thermoelectric device pattern: perpendicular (PERP) or parallel (PARA) to the longer axis of the device. Blue area represents the part of the patterned 30 μm × 1 mm device and yellow area represents the bundles of coated Au nanorod arrays, which cover entire blue-colored device surface. b) The PTE voltage as a function of magnetization angle θ with respect to the x-direction on the x–y plane for the samples with PERP (red) and PARA (blue) alignments. The black symbols represent the results for a control sample without Au nanorods. Here, a magnetic field of 1000 Oe was applied and the linear polarization of light incidence $\vec{E}$ (red arrow) was aligned to the longer axis of the device. c) The same measurement as in panel (b) performed after rotating the sample by 90°, in which voltage probes are along the x-direction (V_x).

laser are matched to the plasmon resonance condition of the Au nanorods. This allows our device to detect the light and its polarization state. Through simulations, we attribute the enhanced PTE signal to the increase in optical absorption and, thereby, the increase in temperature gradient. Our results demonstrate the feasibility of our hybrid structure of ultrathin spin thermoelectric layers with a plasmonic absorber as a PTE-based photodetector.

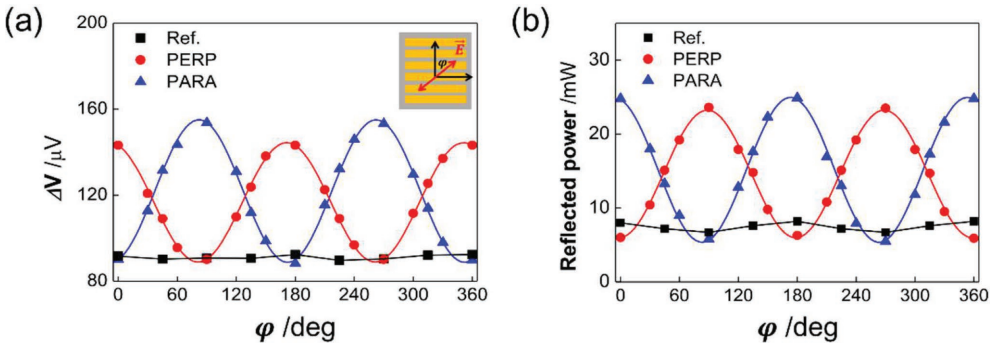

Figure 4. Polarization dependence of the PTE signal. a) PTE voltage ΔV and b) reflected power versus the polarization angle φ. Here, φ is the $\vec{E}$ polarization angle with respect to the longer axis of the device, which is controlled using a zero-order half-wave plate.

4. Experimental Section

Thermoelectric Device Preparation: The bilayers consisting of $Co_{32}Fe_{48}B_{20}$ (CoFeB, 8 nm)/Pt (3 nm) film were prepared on thermally oxidized Si substrates through magnetron sputtering at a base pressure less than 1×10^{-8} Torr and at a working pressure of 3 mTorr. Note that all the samples had a capping layer of MgO (1 nm)/Ta (1.5 nm) that prevented the oxidation of the bilayers. By using photolithography and Ar ion milling, the CoFeB/Pt bilayers were patterned into a 30 μm × 1 mm length bar-shaped structure with two contact pads for an electric measurement. Thereafter, on top of the pattern, parallel arrays of Au nanorods were formed through the solvent-assisted nanotransfer method.[25,26]

Formation of Plasmonic Nanostructure Using Solvent-Assisted Nanotransfer Printing: Au nanorod plasmonic nanostructures were fabricated on a polymer replica layer made from a sub-20 nm SiO_x master template using glancing-angle thermal evaporation with an angle of 75°. The Au deposited polymer replica was then exposed to the mixed vapor of acetone/heptane (1:1 by volume) for 30 s using a preheated solvent chamber at 45 °C. Then, the replica films were placed on the thermoelectric device with a mild pressure for a uniform contact between the substrate and the replica. The printed polymer replica was washed away with a toluene solvent, forming well-aligned plasmonic nanostructures on the thermoelectric device. Note that this method is useful for making a nanoscale structure of tens of nanometers in a large scale.[25]

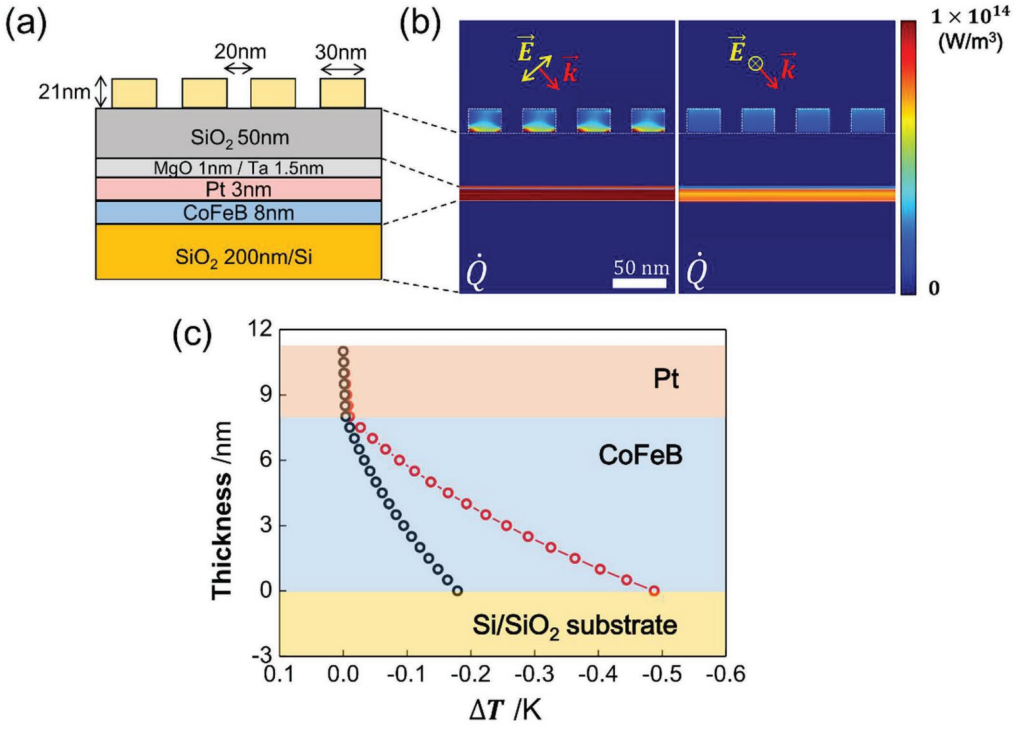

Figure 5. Simulated light absorption and thermal gradient. a) Schematic representation of the sample structure for the simulations. b) Heat production ($\dot{Q}$) profiles due to the absorption of light. The left and right figures correspond to the incident light polarization perpendicular and parallel to the rods, respectively. $\vec{E}$ denotes the electric field of incident light and $\vec{k}$ represents the wave vector, where the incident angle is identical to the experimental condition. c) Temperature-difference (ΔT) profiles of CoFeB/Pt for incident light polarization perpendicular (red) and parallel (black) to the rods.

Optical Absorption Spectra Measurement: The absorption spectra of CoFeB/Pt bilayers with and without an Au nanorod array on a glass substrate, together with a sample consisting of Au nanorod array on a glass substrate were measured by a UV–vis spectrometer (Optizen POP, Mecasys). The measurement range was 400–1000 nm and a glass substrate was used as a reference for the absorption measurement.

Laser-Induced Spin Thermoelectric Measurement: A vertical temperature gradient within the sample was generated by illuminating a linearly polarized laser with a wavelength of 660 or 830 nm. The laser of 5 μm in diameter was focused at the center of the 30 μm × 1 μm bar-shaped device by controlling the focal length of an objective lens. In the setup, the numerical aperture was 0.18, which was believed to be low enough to rule out multiple modes of plasmon excitations.[32] Thermoelectric voltage was measured using two different configurations; i) sweeping a magnetic field between ± 100 Oe in the direction normal to both to temperature gradient and voltage probe and ii) rotating a magnetic field of 1000 Oe on the *x*–*y* plane of the sample. The linear polarization of the laser was controlled by using 660 nm zero-order half-wave plate. All thermoelectric measurements were performed at the room temperature and more than three samples were measured for each type of sample; data were qualitatively reproducible. The error bar represented the standard deviation of 99% confidence interval.

Supporting Information

Supporting Information is available from the Wiley Online Library or from the author.

Acknowledgements

C.-Y.J. and K.M.B. contributed equally to this work. This work was supported by the National Research Foundation of Korea (NRF-2017R1A2A2A05069760, 2017M2A2A6A01071238). S.K. and M.S.J. acknowledge support from Creative Materials Discovery Program through the NRF funded by Ministry of Science and ICT (2016M3D1A1900038).

Conflict of Interest

The authors declare no conflict of interest.

Keywords

light-energy conversion, photothermoelectric effects, plasmonic nanostructures, spin thermoelectric effects

Received: April 29, 2018
Revised: July 4, 2018
Published online:

[1] Y. Pan, G. Tagliabue, H. Eghlidi, C. Höller, S. Dröscher, G. Hong, D. Poulikakos, *Sci. Rep.* **2016**, *6*, 37564.
[2] S. Limpert, A. M. Burke, I.-J. Chen, N. Anttu, S. Lehmann, S. Fahlvik, S. Bremner, G. J. Conibeer, C. Thelander, M.-E. Pistol, *Nano Lett.* **2017**, *17*, 4055.
[3] T. J. Echtermeyer, P. Nene, M. Trushin, R. V. Gorbachev, A. L. Eiden, S. Milana, Z. Sun, J. Schliemann, E. Lidorikis, K. S. Novoselov, *Nano Lett.* **2014**, *14*, 3733.
[4] X. He, X. Wang, S. Nanot, K. Cong, Q. Jiang, A. A. Kane, J. E. Goldsmith, R. H. Hauge, F. o. Léonard, J. Kono, *ACS Nano* **2013**, *7*, 7271.
[5] K. W. Mauser, S. Kim, S. Mitrovic, D. Fleischman, R. Pala, K. Schwab, H. A. Atwater, *Nat. Nanotechnol.* **2017**, *12*, 770.
[6] X. Chen, S. N. Girard, F. Meng, E. Lara-Curzio, S. Jin, J. B. Goodenough, J. Zhou, L. Shi, *Adv. Energy Mater.* **2014**, *4*, 1400452.
[7] A. Zhou, T. Zhu, X. Zhao, S. Yang, T. Dasgupta, C. Stiewe, R. Hassdorf, E. J. Mueller, *Electron Mater.* **2010**, *39*, 2002.
[8] I. Chikina, V. Shikin, A. Varlamov, *Phys. Rev. E* **2012**, *86*, 011505.
[9] P. Mondal, R. Okazaki, H. Taniguchi, I. J. Terasaki, *Appl. Phys.* **2013**, *114*, 173710.
[10] Y.-A. Yan, S. J. Cai, *Chem. Phys.* **2014**, *141*, 054105.
[11] K. Uchida, S. Takahashi, K. Harii, J. Ieda, W. Koshibae, K. Ando, S. Maekawa, E. Saitoh, *Nature* **2008**, *455*, 778.
[12] K. Uchida, H. Adachi, T. Ota, H. Nakayama, S. Maekawa, E. Saitoh, *Appl. Phys. Lett.* **2010**, *97*, 172505.
[13] A. Kirihara, K. Uchida, Y. Kajiwara, M. Ishida, Y. Nakamura, T. Manako, E. Saitoh, S. Yorozu, *Nat. Mater.* **2012**, *11*, 686.
[14] H. A. Atwater, A. Polman, *Nat. Mater.* **2010**, *9*, 205.
[15] C. Hägglund, M. Zäch, G. Petersson, B. Kasemo, *Appl. Phys. Lett.* **2008**, *92*, 053110.
[16] B. P. Rand, P. Peumans, S. R. Forrest, *J. Appl. Phys.* **2004**, *96*, 7519.
[17] H. Chen, L. Shao, Q. Li, J. Wang, *Chem. Soc. Rev.* **2013**, *42*, 2679.
[18] C. L. Haynes, R. P. Van Duyne, *J. Phys. Chem. B* **2001**, *105*, 5599.
[19] P. N. Njoki, I.-I. S. Lim, D. Mott, H.-Y. Park, B. Khan, S. Mishra, R. Sujakumar, J. Luo, C.-J. Zhong, *J. Phys. Chem. C* **2007**, *111*, 14664.
[20] P. Berini, *Phys. Rev. B* **2000**, *61*, 10484.
[21] J. Dionne, L. Sweatlock, H. Atwater, A. Polman, *Phys. Rev. B* **2006**, *73*, 035407.
[22] N. J. Hogan, A. S. Urban, C. Ayala-Orozco, A. Pimpinelli, P. Nordlander, N. J. Halas, *Nano Lett.* **2014**, *14*, 4640.
[23] G. Baffou, P. Bon, J. Savatier, J. Polleux, M. Zhu, M. Merlin, H. Rigneault, S. Monneret, *ACS Nano* **2012**, *6*, 2452.
[24] J. Qiu, W. D. Wei, *J. Phys. Chem. C* **2014**, *118*, 20735.
[25] J. W. Jeong, S. R. Yang, Y. H. Hur, S. W. Kim, K. M. Baek, S. Yim, H.-I. Jang, J. H. Park, S. Y. Lee, C.-O. Park, Y. S. Jung, *Nat. Commun.* **2014**, *5*, 5387.
[26] J. W. Jeong, M. M. P. Arnob, K. M. Baek, S. Y. Lee, W. C. Shih, Y. S. Jung, *Adv. Mater.* **2016**, *28*, 8695.
[27] G. Armelles, J. B. González-Díaz, A. García-Martín, A. García-Martín, J. M. García-Martín, A Cebollada, M. U. González, S. Acimovic, J. Cesario, R. Quidant, G. Badenes, *Opt. Express* **2008**, *16*, 16104.
[28] D.-J. Kim, S.-I. Kim, S.-Y. Park, K.-D. Lee, B.-G. Park, *Curr. Appl. Phys.* **2014**, *14*, 1344.
[29] K.-D. Lee, D.-J. Kim, H. Y. Lee, S.-H. Kim, J.-H. Lee, K.-M. Lee, J.-R. Jeong, K.-S. Lee, H.-S. Song, J.-W. Sohn, S.-C. Shin, B.-G. Park, *Sci. Rep.* **2015**, *5*, 10249.
[30] D.-J. Kim, K.-D. Lee, S. Surabhi, S.-G. Yoon, J.-R. Jeong, B.-G. Park, *Adv. Funct. Mater.* **2016**, *26*, 5507.
[31] K. Uchida, H. Adachi, D. Kikuchi, S. Ito, Z. Qiu, S. Maekawa, E. Saitoh, *Nat. Commun.* **2015**, *6*, 5910.
[32] A. S. Hall, M. Faryad, G. D. Barber, L. Liu, S. Erten, T. S. Mayer, A. Lakhtakia, T. E. Mallouk, *ACS Nano* **2013**, *7*, 4995.